Journal of Applied Electrochemistry (2007) 37:15–20
DOI 10.1007/s10800-006-9215-y

Electrochemical characterization of perovskite-based SOFC cathodes

S. BEBELIS[1,*], N. KOTSIONOPOULOS[1], A. MAI[2] and F. TIETZ[2]
[1]*Department of Chemical Engineering, University of Patras, Patras, GR-26504, Greece*
[2]*Institute for Materials and Processes in Energy Systems (IWV-1), Forschungszentrum Jülich, D-52425, Jülich, Germany*
*(*author for correspondence, tel.: + 30-2610-969512, fax: + 30-2610-997269, e-mail: simeon@chemeng.upatras.gr)*

Received 14 February 2006; accepted in revised form 23 May 2006

Key words: cathodes, composite electrodes, LSCF, LSM-YSZ, mixed conductors, perovskites, SOFC, solid oxide fuel cells

Abstract

The electrochemical performance of $La_{0.58}Sr_{0.4}Co_{0.2}Fe_{0.8}O_{3-\delta}$ (L58SCF), $La_{0.78}Sr_{0.2}Co_{0.2}Fe_{0.8}O_{3-\delta}$ (L78SCF) and composite $La_{0.65}Sr_{0.3}MnO_{3-\delta}$ – 8 mol% Y_2O_3 stabilized ZrO_2 (LSM-YSZ, 50:50 wt%) cathode electrodes interfaced to a double-layer electrolyte made of $Ce_{0.8}Gd_{0.2}O_{2-\delta}$ (CGO) and YSZ was studied in the temperature range 600–850 °C using impedance spectroscopy and current-overpotential measurements. The experiments were carried out in a single chamber cell using a three electrode set-up with porous Pt films as auxiliary electrodes. The perovskite powders were synthesized using the spray-drying technique starting from nitrate precursors and were deposited on the solid electrolyte via screen-printing. Open circuit impedance measurements on as-prepared electrodes, i.e. before any polarization, and micropolarization measurements have shown that the L78SCF/CGO/YSZ electrode exhibits the lowest area specific polarization resistance R_F (R_F was approximately equal to 0.4 Ω cm^2 at 800 °C and P_{O_2} = 21 kPa) or, equivalently, the highest electrocatalytic activity according to the order: LSM/LSM-YSZ/CGO/YSZ < L58SCF/CGO/YSZ < L78SCF/CGO/YSZ. Current-overpotential data taken over an extended cathodic overpotential (ohmic-drop-free) range (0 to −500 mV) also indicated the aforementioned order of electrocatalytic activity. The Nyquist plots corresponded to at least two overlapping arcs or, equivalently, to at least two rate limiting processes. The relative contribution and degree of overlap of these arcs depended on electrode material, temperature and oxygen partial pressure, the low frequency arc being in general dominant at low temperatures and low oxygen partial pressures. Open circuit impedance experiments carried out at different oxygen partial pressures P_{O_2} (0.01–100 kPa) revealed an exponential increase of the open-circuit area specific polarization conductance R_F^{-1} with increasing P_{O_2}.

1. Introduction

Commercialization of intermediate temperature (600–800 °C) solid oxide fuel cells (SOFCs) requires the development of new cathode electrodes with high electrocatalytic activity for oxygen reduction, as below 800 °C the performance of conventional cathodes based on $La_{1-x}Sr_xMnO_{3-\delta}$ (LSM) is not satisfactory. Promising alternatives to these electrodes are composite electrodes made of a perovskite with a solid electrolyte, e.g. LSM-$ZrO_2(Y_2O_3)$ electrodes [1, 2], which behave effectively as mixed conductors on the macroscopic scale [3], as well as mixed ionic-electronic conducting electrodes, e.g. $La_{0.8}Sr_{0.2}FeO_{3-\delta}$ [4] or $La_{1-x-y}Sr_xCo_{0.2}Fe_{0.8}O_{3-\delta}$ (x = 0.2 and 0.4; y = 0–0.05) [5] electrodes. In addition to a high electronic conductivity, these electrodes exhibit high oxygen ion conductivity [4, 6, 7] which is expected to result in enlargement of the area where oxygen reaction can take place [8, 9] and to high oxygen surface exchange coefficients for faster kinetics at the gas/cathode interface [10]. The evaluation of the electrochemical performance of these electrodes as cathodes in SOFCs is usually based on the current density–voltage curves of single cells where the same anode is used [5], but also on the individual polarization and impedance characteristics of the cathodes, which directly correlate with their electrocatalytic activity. Most of the latter studies concern the electrochemical performance of LSM-$ZrO_2(Y_2O_3)$ composite cathodes [1, 11–16], while fewer studies have appeared concerning the electrochemical performance of iron- and cobalt-containing perovskite cathodes, e.g. $La_{1-x}Sr_xCo_{1-y}Fe_yO_{3-\delta}$ (LSCF) [9, 17–21] cathodes. In the present work electrochemical characterization is carried out on a LSM-$ZrO_2(Y_2O_3)$ composite cathode and two A-site deficient LSCF cathodes interfaced to the $Ce_{0.8}Gd_{0.2}O_{2-\delta}$ (CGO) layer of a double layer $Ce_{0.8}Gd_{0.2}O_{2-\delta}/ZrO_2$ (8 mol% Y_2O_3), or CGO/8YSZ, electrolyte, using impedance

spectroscopy and steady state current density–overpotential measurements. A double layer CGO/8YSZ electrolyte is normally used in the case of ferrite-based cathodes in order to prevent chemical reactions between the cathode and the YSZ electrolyte [5, 22].

2. Experimental details

The experiments were carried out in a single chamber cell in the temperature range 600–850 °C. A three electrode set-up was used, with porous Pt films as auxiliary (counter and reference) electrodes. The auxiliary electrodes were deposited on one side of a 8YSZ disk. The counter electrode was positioned exactly opposite to the perovskite or composite electrode (working electrode) in order to obtain an optimal distribution of current lines. The latter was deposited on the other side of the disk, interfaced to a CGO layer deposited on the 8YSZ disk. A schematic of the cell and of the electrode set-up is shown in Figure 1. The cell had a volume of approximately 30 cm^3 and was made of a quartz tube closed at one end. The open end of the tube was mounted on a stainless steel cap. The 8YSZ disk was clamped inside the quartz tube using gold wires pressed on it between two non-conductive ceramic (Macor) slabs. These gold wires also connected the electrodes with the external electric circuit. In the case of the perovskite or composite working electrode, a platinum gauze (52 mesh) pressed on the electrode and connected to the gold wire was used as current collector.

The perovskite powders were synthesized using the spray-drying technique starting from nitrate precursors [23, 24] and they were calcined at 900 °C in order to develop the perovskite phase [24]. The stoichiometry of the powders was controlled by optical emission spectroscopy (ICP-OES), while the phase composition was evaluated by X-ray diffraction [5, 24]. After calcination of the powders, they were ground by ball milling for several hours. The mixed conducting materials L78SCF and L58SCF (Table 1) were ground until a mean particle size (d_{50}) of approximately 0.8 μm was obtained. The composite cathode LSM-YSZ was made of 50 wt% 8YSZ powder (Tosoh, Japan) ground to a d_{50} of approximately 0.4 μm and 50 wt% $La_{0.65}Sr_{0.3}MnO_{3-\delta}$ (LSM) powder ground to approximately 0.5 μm. The CGO powder (Treibacher Auermet, Austria) was also ground by ball milling. Screen printing was used for the deposition of the perovskite and composite electrodes, which were then sintered at 1060 or 1100 °C. The composite electrode functional layer was coated via screen printing with a coarse current collector layer consisting of unground LSM (d_{50} = 12 μm). The CGO layer was deposited on 8YSZ also using screen printing followed by sintering at 1300 °C for 3 h. The pastes used for screen printing were prepared from the corresponding powders by mixing with an ethyl cellulose binder and a terpineol-based solvent. The abbreviations used hereafter, the composition and the preparation data of the tested electrodes are listed in Table 1. Their geometric area was equal to approximately 1.6 cm^2. The two auxiliary porous Pt electrode films were prepared applying thin layers of a Pt organometallic paste (Engelhard-CLAL M603B) on the YSZ disk, followed by calcining first at 400 °C for 2 h and then at 850 °C for 30 min. The geometric area of the counter electrode was 1.5–1.6 cm^2 and the one of the reference electrode equal to 0.5–0.6 cm^2.

Characterization of the microstructure of the electrodes was performed using scanning electron microscopy (LEO SUPRA 35VP). Figure 2 shows scanning electron micrographs of top views of the electrodes and of sections perpendicular to the electrode/electrolyte interface. The electrochemical characterization was carried out using a Princeton Applied Research 263A potentiostat combined with a Princeton Applied Research 5210 dual phase lock-in amplifier for performing AC impedance measurements. The amplitude of the applied stimulus was 10 mV. The 263A/5210 system was controlled by the PowerSuite software package (Princeton Applied Research). Comparisons among the different electrodes concerning their electrocatalytic activity were carried out under flow of 21% O_2/He mixture (flow rate 100–200 cm^3 (STP) min^{-1}) and were two-fold: First, the electrodes were compared on the basis of the corresponding polarization conductance under open circuit conditions determined from AC impedance measurements. Initial comparison was based on the electrodes as prepared, i.e. before polarization, in order to exclude the possibility of changes induced in the electrodes by polarization. Secondly, the electrodes were compared on the basis of the current density passing through the electrode/electrolyte interface for the same ohmic-drop free cathodic overpotential. The ohmic

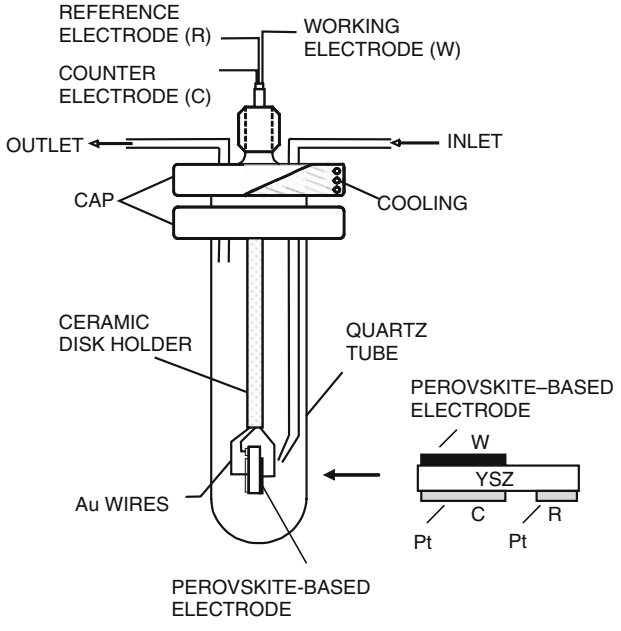

Fig. 1. Schematic of the test cell and of the electrode set-up.

Table 1. Composition and preparation data of the tested electrodes

Electrode	Electrode composition	Electrolyte	Sintering temperature /sintering time
L78SCF/CGO/YSZ	$La_{0.78}Sr_{0.2}Co_{0.2}Fe_{0.8}O_{3-\delta}$	CGO/8YSZ[b]	1060 °C (3 h)
L58SCF/CGO/YSZ	$La_{0.58}Sr_{0.4}Co_{0.2}Fe_{0.8}O_{3-\delta}$	CGO/8YSZ[a]	1100 °C (3 h)
LSM/LSM-YSZ/CGO/YSZ	$La_{0.65}Sr_{0.3}MnO_{3-\delta}$/LSM-8YSZ (50 wt% LSM –50 wt% 8YSZ)	CGO/8YSZ[a]	1100 °C (3 h)

[a]Commercial (Kerafol) 8YSZ disk (0.4–0.5 mm thickness, 20 mm diameter).
[b]8YSZ disk prepared by pressing 8YSZ power (Tosoh, pressure 70 kN) and then sintering at 1500 °C for 5 h (1 mm thickness, 20 mm diameter).

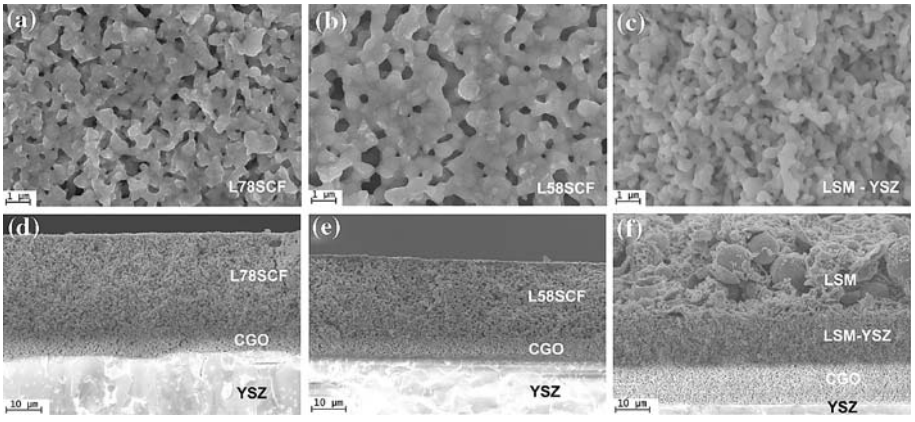

Fig. 2. Scanning electron micrographs of the tested cathodes (Table 1). (a, b): top view; (c–f): cross section perpendicular to the cathode/electrolyte interface.

component of the overpotential was automatically determined during potential scan (sweep rate 0.1 mV s^{-1}) using the current interruption technique [25]. Before the series of the current vs. overpotential experiments the electrodes were pretreated by sequential application at 800 °C of −200 mA for 2 h and −500 mA for 30 min, in order to stabilize their electrocatalytic activity. In the case of the LSM-YSZ composite electrode open circuit impedance measurements were also carried out under different oxygen partial pressures (0.01–100 kPa).

3. Results and discussion

3.1. *Impedance characteristics at $P_{O_2} = 21$ kPa*

The impedance characteristics of the electrodes (Table 1) are compared at four different temperatures (600–750 °C) at $P_{O_2} = 21$ kPa and in the form of Nyquist plots in Figure 3. The impedance spectra correspond to at least two overlapping depressed arcs, or, equivalently, the impedance characteristics are determined by at least two different processes, such as bulk or surface diffusion or surface exchange of oxygen and charge transfer [3, 18]. The relative magnitude of these depressed arcs and the degree of overlapping depends on the electrode but also on temperature. In the case of the LSCF electrodes, the arc corresponding to low frequencies becomes dominant with decreasing temperature, while in the case of the LSM/LSM-YSZ electrode the high frequency arc remains dominant at all temperatures. Concerning the magnitude of the polarization resistance, the L78SCF electrode clearly exhibits the lowest polarization resistance over the whole temperature range.

This is better shown in Figure 4 where the open circuit area specific apparent polarization conductances R_F^{-1} (expressed in Ω^{-1} cm^{-2}) of all tested electrodes, determined from the open circuit impedance measurements (Figure 3), are compared at different temperatures (600–850 °C) in the form of an Arrhenius plot. It is noted that R_F is determined by the intersection of each impedance spectrum in the Nyquist plots with the Z_{re} axis. On the basis of open-circuit impedance data (Figures 3 and 4) it is concluded that over the whole temperature range 600–850 °C and at $P_{O_2} = 21$ kPa the L78SCF/CGO/YSZ electrode exhibits the lowest area specific polarization resistance R_F (approximately equal to 0.4 Ω cm^2 at 850 °C) or, equivalently, the highest polarization conductance. This means that it also exhibits the highest electrocatalytic activity according to the order LSM/LSM-YSZ/CGO/YSZ < L58SCF/CGO/YSZ < L78SCF/CGO/YSZ. The activation energy E_a values for all electrodes (Figure 4) do not differ substantially, varying between 1.15 and 1.47 eV, which may imply a similar mechanism for oxygen reduction, at least near open circuit. The measured E_a values are in good agreement with those reported in prior studies. Activation energies from 1.38 to 1.65 eV have been reported [3, 18, 20, 26] for $La_{0.6}Sr_{0.4}Co_{0.2}Fe_{0.8}O_{3-\delta}$/CGO cathodes sintered at 850–1000 °C for 2–4 h, while an activation energy of

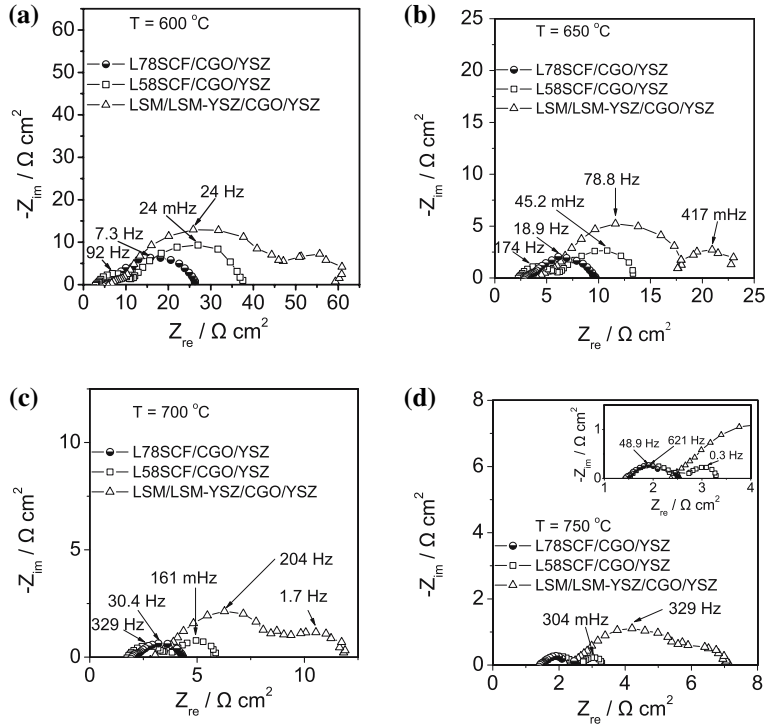

Fig. 3. Comparison of the open circuit impedance characteristics of the L78SCF/CGO/YSZ (100 mHz–100 kHz), L58SCF/CGO/YSZ (1 mHz–100 kHz) and LSM/LSM-YSZ/CGO/YSZ (10 mHz–100 kHz) electrodes at P_{O_2} = 21 kPa. (a) 600 °C (b) 650 °C (c) 700 °C (d) 750 °C.

1.04 eV has been reported for LSM-YSZ/YSZ cathodes [12] sintered at 1000 °C for 2 h.

3.2. *Polarization characteristics at $P_{O_2} = 21$ kPa*

In order to compare the electrocatalytic activity of the cathodes under conditions similar to those under fuel cell operation, the current densities i corresponding to the same overpotential η were compared at different temperatures over an extended cathodic overpotential range. Figure 5 shows the dependence of current density i on the ohmic-drop-free overpotential η for all electrodes in the form of semilogarithmic plots (Tafel plots), compared at four different temperatures (600–750 °C). The conclusion drawn from these Tafel plots is that at the same temperature and overpotential and over the entire temperature and electrode overpotential range the current densities increase in the order LSM/LSM-YSZ/CGO/YSZ < L58SCF/CGO/YSZ < L78SCF/CGO/YSZ. This order also represents the order of electrocatalytic activity and is in agreement with the conclusions drawn from the open circuit impedance measurements (Figures 3 and 4). In mixed conductors the competition between bulk and surface pathways for oxygen reduction [27] and the difference between the applied overpotential and the change in electrostatic potential at the electrode/gas interface [28] can obscure the meaning of the electrokinetic parameters obtained from conventional Tafel analysis of the current density vs. overpotential data. In view of this, no such analysis was attempted here.

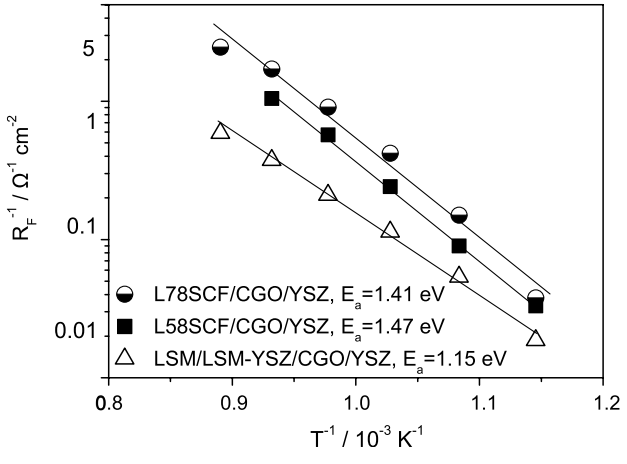

Fig. 4. Comparison of the open circuit polarization conductances R_F^{-1} of the electrodes at different temperatures (Arrhenius plot).

The observed differences in electrocatalytic activity can be attributed to a large extent to differences in microstructure and ionic conductivity, as these factors determine the area where oxygen reduction can take place and the kinetics of the surface exchange of oxygen [5, 10, 29]. It has been recently reported [5] that the electrocatalytic performance for oxygen reduction of $La_{1-x-y}Sr_xCo_{0.2}Fe_{0.8}O_{3-\delta}$ (x = 0.2 and 0.4; y = 0–0.05) electrodes is significantly higher than that of state-of-the-art LSM/LSM-YSZ/YSZ electrodes with similar microstructure, on the basis of current densities obtained in corresponding planar anode-supported

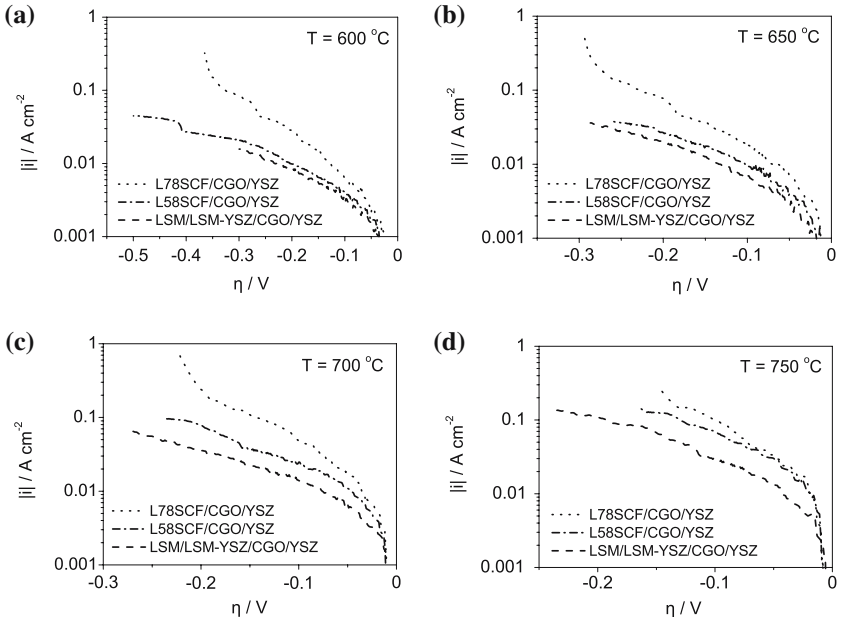

Fig. 5. Dependence of current density i on ohmic-drop-free overpotential η (Tafel plots) and on temperature at P_{O_2} = 21 kPa. (a) 600 °C (b) 650 °C (c) 700 °C (d) 750 °C.

SOFCs. This is in agreement with the results of the present study, where it was found that LSCF cathodes exhibit a higher electrocatalytic activity compared to LSM/LSM-YSZ electrodes interfaced to the CGO layer of a double layer CGO/8YSZ electrolyte. As shown in Table 1, the L78SCF cathode, which exhibited the highest electrocatalytic activity, was sintered at a temperature by 40 °C lower than that used in the case of the other two tested electrodes. Lowering of the sintering temperature results, in general, in a higher specific surface area of the cathode and therefore to a larger number of active sites. This partly explains why the L78SCF cathode exhibited a higher electrocatalytic activity compared to the L58SCF cathode (both electrode materials have the same A-site deficiency), in contrast to the results reported by Mai et al. [5], where the better performance of the L58SCF cathode was attributed to the higher Sr content and the corresponding larger number of oxygen vacancies and electronic holes [10, 30, 31] which improves conductivity and surface exchange of oxygen. Indeed, as shown in Figure 2, the L58SCF electrode has a slightly coarser microstructure compared to the L78SCF electrode.

3.3. *Effect of oxygen partial pressure on the impedance characteristics of the LSM/LSM-YSZ electrode*

The effect of oxygen partial pressure P_{O_2} (0.01–100 kPa) on the impedance characteristics was studied under open circuit conditions for the LSM/LSM-YSZ/CGO/YSZ electrode. The experiments were carried out after the polarization experiments (Figure 5). As shown in Figure 6a, for T = 750 °C, the oxygen partial pressure significantly affects the relative contribution and overlapping of the depressed arcs which constitute the Nyquist plots, mostly affecting the low frequency arc. The latter becomes dominant at low oxygen partial pressures. Similar behavior was also observed at other temperatures. Figure 6(b) presents the effect of oxygen partial pressure on the open circuit polarization conductance, determined from open-circuit impedance measurements (Figure 6(a)). Polarization conductance increases with increasing P_{O_2}, following an apparent power law dependence $R_F^{-1} = k P_{O_2}^n$ with $n \approx 0.2$. A similar dependence of R_F^{-1} on oxygen partial pressure, corresponding mostly to values of the exponent n between 0.3 and 0.6, has been reported in previous studies of LSM-YSZ/YSZ cathodes [1, 13, 15, 16], where various explanations were proposed to account for this effect. The dependence of R_F^{-1} on P_{O_2} found in the present work is close to the $P_{O_2}^{0.29}$ dependence reported by Murray et al. [16] and associated with oxygen dissociation and adsorption limiting steps and to the $P_{O_2}^{0.25}$ dependence reported by Kim et al. [15] and associated via modeling with O^- surface diffusion from adsorption sites to the three phase boundary region.

4. Conclusions

The impedance and polarization characteristics of A-site deficient iron- and cobalt-containing (LSCF) perovskite and composite $La_{0.65}Sr_{0.3}MnO_{3-\delta}/ZrO_2$ (8 mol% Y_2O_3) (LSM-YSZ) cathodes interfaced to the $Ce_{0.8}Gd_{0.2}O_{2-\delta}$ (CGO) layer of a double layer CGO/8YSZ electrolyte were compared. The electrodes had similar but not exactly the same microstructure. The highest electrocatalytic activity for oxygen reduction was observed for the $La_{0.78}Sr_{0.2}Co_{0.2}Fe_{0.8}O_{3-\delta}$

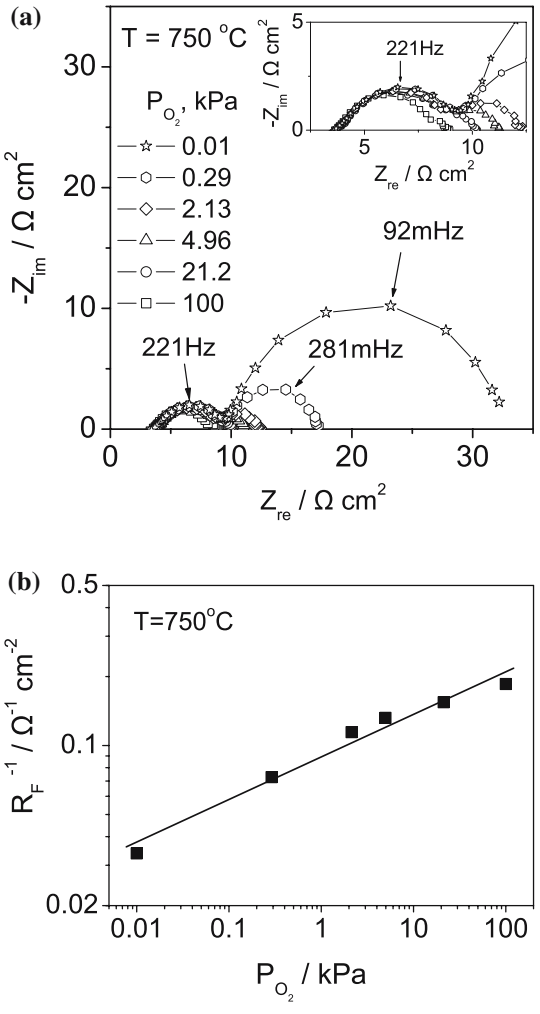

Fig. 6. Dependence of the open circuit impedance characteristics of the LSM/LSM-YSZ/CGO/YSZ cathode on oxygen partial pressure P_{O_2}. T = 750 °C. Frequency range: 10 mHz–100 kHz (a) Nyquist plots at different oxygen partial pressures P_{O_2} (b) Effect of oxygen partial pressure P_{O_2} on open circuit polarization conductance R_F^{-1}.

(L78SCF) cathode, according to the order LSM/LSM-YSZ/CGO/YSZ < $La_{0.58}Sr_{0.4}Co_{0.2}Fe_{0.8}O_{3-\delta}$/CGO/YSZ < $La_{0.78}Sr_{0.2}Co_{0.2}Fe_{0.8}O_{3-\delta}$/CGO/YSZ.

Acknowledgements

The authors gratefully acknowledge financial support by the Greek-German bilateral scientific-technical collaboration programme (GRC 01/99), the "C. Caratheodory" Programme (Research Committee, Univ. of Patras) and the Integrated Project "Real-SOFC" (Project No: SES6-CT-2003-502612). They also thank Dr V. Drakopoulos, Institute of Chemical Engineering and High Temperature Chemical Processes (ICE-HT/FORTH) for the scanning electron microscopy characterization of the electrodes.

References

1. M.J. Jørgensen and M. Mogensen, *J. Electrochem. Soc.* **148** (2001) A433.
2. T. Kenjo and M. Nishiya, *Solid State Ionics* **57** (1992) 295.
3. V. Dusastre and J.A. Kilner, *Solid State Ionics* **126** (1999) 163.
4. S.P. Simner, J.F. Bonnett, N.L. Canfield, K.D. Meinhardt, V.L. Sprenkle and J.W. Stevenson, *Electrochem. Solid State Lett.* **5** (2002) A173.
5. A. Mai, V.A.C. Haanappel, S. Uhlenbruck, F. Tietz and D. Stöver, *Solid State Ionics* **176** (2005) 1341.
6. Y. Teraoka, H.M. Zhang, K. Okamoto and N. Yamazoe, *Mater. Res. Bull.* **23** (1988) 51.
7. J.W. Stevenson, T.R. Armstrong, R.D. Carneim, L.R. Pederson and W.J. Weber, *J. Electrochem. Soc.* **143** (1996) 2722.
8. J. Fleig, *J. Power Sources* **105** (2002) 228.
9. S.B. Adler, J.A. Lane and B.C.H. Steele, *J. Electrochem. Soc.* **143** (1996) 3554.
10. J.A. Kilner, R.A. De Souza and I.C. Fullarton, *Solid State Ionics* **86–88** (1996) 703.
11. A.C. Co, S.J. Xia and V.I. Birss, *J. Electrochem. Soc.* **152** (2005) A570.
12. A. Barbucci, R. Bozzo, G. Cerisola and P. Costamagna, *Electrochim. Acta* **47** (2002) 2183.
13. S. Wang, Y. Jiang, Y. Zhang, J. Yan and W. Li, *Solid State Ionics* **113–115** (1998) 291.
14. A. Barbucci, P. Carpanese, G. Gerisola and M. Viviani, *Solid State Ionics* **176** (2005) 1753.
15. J-D. Kim, G.-D. Kim, J.-W. Moon, Y.-I. Park, H.-W. Lee, K. Kobayashi, M. Nagai and C.-E. Kim, *Solid State Ionics* **143** (2001) 379.
16. E. Perry Murray, T. Tsai and S.A. Barnett, *Solid State Ionics* **110** (1998) 235.
17. D.Z. de Florio, R. Muccillo, V. Esposito, E. Di Bartolomeo and E. Traversa, *J. Electrochem. Soc.* **152** (2005) A88.
18. E. Perry Murray, M.J. Sever and S.A. Barnett, *Solid State Ionics* **148** (2002) 27.
19. H.Y. Tu, Y. Takeda, N. Imanishi and O. Yamamoto, *Solid State Ionics* **117** (1999) 277.
20. A. Esquirol, N.P. Brandon, J.A. Kilner and M. Mogensen, *J. Electrochem. Soc.* **151** (2004) A1847.
21. N. Grunbaum, L. Dessemond, J. Fouletier, F. Prado and A. Caneiro, *Solid State Ionics* **177** (2006) 907.
22. A. Tsoga, A. Gupta, A. Naoumidis and P. Nikolopoulos, *Acta Mater.* **48** (2000) 4709.
23. P. Kountouros, R. Förthmann, A. Naoumidis, G. Stochniol and E. Syskakis, *Ionics* **1** (1995) 40.
24. A. Mai, PhD Thesis, Ruhr-Univ. Bochum, Schriften des Forschungszentrum Jülich, Energietechnik, Vol. 31 (2004).
25. Technical Note 101: Potential Error Correction (iR Compensation), Princeton Applied Research (PAR) (Oak Ridge, TN, 1986).
26. D. Waller, J.A. Lane, J.A. Kilner and B.C.H. Steele, *Solid State Ionics* **86–88** (1996) 767.
27. G.W. Coffey, L.R. Pederson and P.C. Rieke, *J. Electrochem. Soc.* **150** (2003) A1139.
28. J. Fleig, *Phys. Chem. Chem. Phys.* **7** (2005) 2027.
29. J. Fleig and J. Maier, *J. European Ceramic Soc.* **24** (2004) 1343.
30. H. Ullmann, N. Trofimenko, F. Tietz, D. Stöver and A. Ahmad-Khanlou, *Solid State Ionics* **138** (2000) 79.
31. A. Mai, F. Tietz and D. Stöver, *Solid State Ionics* **173** (2004) 35.